RSC Advances

PAPER

View Article Online
View Journal | View Issue

Cite this: *RSC Adv.*, 2021, **11**, 10635

Investigation on the transformation behaviours of Fe-bearing minerals of coal in O_2/CO_2 combustion atmosphere containing H_2O

Fang Huang, *[a] Shanzhi Xin,[a] Tie Mi[a] and Liqi Zhang[b]

The transformation behaviors of Fe-bearing minerals in coals of Xinjiang (XJC) and Shenhua (SHC) were investigated in an O_2/CO_2 atmosphere containing H_2O in a drop-tube-furnace (DTF). The solid products were characterized using XRD, Mössbauer spectroscopy, particle size analyzer and SEM-EDX techniques. The results show that the change in the combustion atmosphere does not significantly alter the main phases of Fe-bearing minerals in the coal ashes, but does affect their relative contents. The ratio of Fe^{2+}-glass to Fe^{3+}-glass in the ashes produced from the O_2/CO_2 combustion atmosphere was significantly increased. During the XJC combustion and under different combustion conditions examined, the content of Fe-glass phases remained almost unaltered. However, in SHC samples, combustion under O_2/CO_2 atmosphere resulted in a higher amount of iron melting into Fe-glass phases and less amount of iron oxide formation. This could be attributed mainly to the presence of Fe-bearing minerals mostly included in nature in SHC samples, which more easily interacted with clays or other silicates inside coal-formed Fe-glass phases. Increasing the O_2 level of the O_2/CO_2 atmosphere during SHC combustion could promote the formation of iron oxides. In O_2/CO_2 atmosphere, with the same oxygen level, the replacement of 10% of CO_2 with H_2O promoted the formation of iron oxides, regardless of the occurrence form (included or excluded) of iron minerals in coal. Furthermore, the addition of steam resulted in an increase in the size of the particles in ash, resulting probably in a decrease in the deposition and slagging propensity of coal ash.

Received 26th January 2021
Accepted 24th February 2021

DOI: 10.1039/d1ra00673h

rsc.li/rsc-advances

1. Introduction

Iron-containing minerals are considered one of the major contributors of deposition, slagging and fouling problems in the pulverized coal combustion process.[1,2] Pyrite, siderite, ankerite and iron-bearing clay minerals, such as Fe^{2+}-illite, are the most common iron-bearing minerals in coal.[3,4] Generally, the ash produced from coal combustion contains iron mainly in the form of magnetite (Fe_3O_4), while iron in the ash deposition on the furnace wall is mainly in the form of hematite (Fe_2O_3).[5] Under coal combustion atmosphere and during the process of migration and transformation, the effects of iron-bearing minerals in different forms on the formation of deposition, slagging and fouling differ significantly. Reductive Fe^{2+}-containing minerals, such as pyrrhotite and wustite, make a greater contribution to the deposition. Iron oxides present in the Fe^{2+} state have a lower melting temperature,[4] while hematite and magnetite in the Fe^{3+} state contributes less to the deposition.[6] When iron is wrapped in silicate ash particles forming Fe-glass silicates, the melting temperature and viscosity of the particles decrease rapidly.[7] At a certain temperature, the formed Fe^{2+}-glass is further oxidized into Fe^{3+}-glass in particles, resulting to an increase in the viscosity. Therefore, the ratio of Fe^{2+}-glass to Fe^{3+}-glass in ash particles plays an important role in determining the tendency of slagging and melting.

Many investigators have studied the transformation characteristics of iron-bearing phases in the air atmosphere.[8–11] Pyrite is generally decomposed to pyrrhotite and then oxidized into magnetite and hematite. Siderite (iron carbonate) is decomposed into wustite, which is then oxidized to magnetite and hematite. If they are encapsulated within a coal particle, pyrite and siderite will form Fe^{2+}-glass and Fe^{3+}-glass silicates through melting of the intermediate products of their transformation, which are bonded to silicates. Fe-containing illite is converted to Fe^{2+}-glass silicate and further converted to Fe^{3+}-glass silicate in an oxidizing environment. During coal combustion, the combustion atmosphere and temperature influence dramatically or to a large extent the migration characteristics of mineral composition.[12] Thus far, O_2/CO_2 combustion is one of the most promising technologies to control and capture CO_2 from coal combustion on a large scale. Due to the great change in the combustion atmosphere, the evolution paths and

[a]*Hubei Key Laboratory of Industrial Fume and Dust Pollution Control, Jianghan University, 8 Sanjiaohu Road, Wuhan 430056, Hubei, P. R. China. E-mail: huangfang5869684@126.com; Fax: +86 027 87546806; Tel: +86 13397112751*

[b]*State Key Laboratory of Coal Combustion, Huazhong University of Science and Technology, 1037 Luoyu Road, Wuhan 430074, Hubei, P. R. China*

transformation behaviors of minerals under the O_2/CO_2 combustion atmosphere follow complicated procedures. Krishnamoorthy and Veranth[13] suggested or proposed that an increase in the CO_2 concentration in the combustion atmosphere can significantly change the ratio of CO to CO_2 in char particles, which will further affect the transformation of the iron-bearing phases. In addition, in O_2/CO_2 atmosphere, the water vapor concentration in the furnace is as high as 18–30 vol%,[14,15] which is much higher (7–10%) than that during the conventional air combustion and even higher than 40% (ref. 16 and 17) of the relevant amount present in the wet cycle. The coal char will be gasified much easier in a higher water vapour content atmosphere.[18] When water vapour and carbon dioxide are both present in the furnace atmosphere, water molecules will primarily occupy active sites in char.[19] In this respect Yadav and Mondal[20] found that the char gasification reaction was enhanced in water vapor enrichment cases, affecting the flame temperature distribution and the incident radiation profile of the combustion furnace. Niu *et al.* also investigated intrinsic kinetics to predict ash effects on coal char burnout in air and O_2/CO_2 atmospheres showing that ash vaporization was lower in O_2/CO_2 atmospheres than in air.[21] In summary, the combustion environment is greatly affected by the addition of water vapor in the combustion atmosphere. Such a high concentration of H_2O in the O_2/CO_2 combustion atmosphere will definitely complicate the migration and evolution of mineral components in coal.

So far, the transformation behaviour of inorganic matters in coal under O_2/CO_2 combustion[22–25] has been extensively studied. Stimpson *et al.* reported that oxy-fuel combustion deposits contained a higher content of sulphur.[22] However, in oxy-coal combustion, in simulation research, where a high O_2 level was used, the mass fraction of submicron particles and initial layer ash deposition were higher due to the involvement of Fe, Ca, Mg, Al, and Si.[23] A few researchers investigated the Fe-bearing mineral in O_2/CO_2 combustion atmosphere. Li *et al.* found that the transformation of iron-bearing minerals in coal, in the process of O_2/CO_2 combustion, is more conducive to the formation of Fe-glass silicates.[12] This has been attributed to the higher iron content in coal, upon the inclusion of pyrite and siderite, resulting in an increase in slag formation. However, Sheng *et al.* and Yu *et al.* suggested that O_2/CO_2 combustion did not promote the Fe-glass silicate formation.[1,2]

At this point, thus far, it should be noted that the influence of the water vapor content on the O_2/CO_2 atmosphere used for the Fe-bearing mineral transformation has been studied rarely. Therefore, in this work, we investigated the transformation characteristics of mineral matters especially iron minerals of Xinjiang (XJC) and Shenhua coal (SHC) during the O_2/CO_2 combustion in a water vapor-containing atmosphere. The ashes after coal combustion were analysed using standard experimental techniques such as X-ray diffraction (XRD), particle size analyser, and scanning electron microscopy with energy dispersive X-ray (SEM-EDX). Moreover, coal ashes from different atmospheres were also analysed by Mössbauer spectroscopy, providing evidence for the distribution and content of Fe-bearing phases. Consequently, the obtained results are providing some new insights about the coal combustion ashes formed during oxy-coal combustion within the wet recycle.

2. Experimental section

2.1. Fuel properties

The coals used in this study are Xinjiang (XJC) and Shenhua coals (SHC). The proximate analysis, ultimate analysis, lower heating value, and total sulphur contents (according to the Chinese standards of GB/T212-2008, GB/T476-2008, GB/T213-2008 and GB/T214-2007) of the coals are shown in Table 1. Each analysis was conducted three times under the same conditions to gain the average value. The ash chemical composition analysis of the coals is also presented in Table 1. Each ash sample was tested by XRF (X-ray fluorescence) to analyse the micro-region composition of three points. The XJC and SHC samples have a medium-low heating value and high volatile matter, suggesting that the two coals belong to the typical low-rank bituminous coals.

2.2. Experimental systems

Combustion experiments were conducted in a drop tube furnace (DTF) and all experiments were carried out at 1450 °C. The experimental system used for this work is shown in Fig. 1.

The whole experimental system consists of four parts: a furnace and its temperature controller, coal particle feeder, gas supply system, and sampling system. The furnace generally can reach the highest temperature of 1450 °C. The corundum tube reactor in the furnace has an inner diameter of 50 mm, an

Table 1 Properties of the coal samples used in the study

Sample	XJC	SHC
Property analysis (wt%, dry basis)		
Moisture	2.11	2.05
Volatile matter	30.95	32.46
Ash	14.45	17.13
Fixed carbon	52.48	48.35
LHV (MJ kg^{-1})	27.8	25.6
Ultimate analysis (wt%, dry basis)		
Carbon	67.03	61.72
Hydrogen	4.20	3.76
Nitrogen	0.96	0.97
Oxygen (diff)	10.25	13.86
Sulphur	1.00	0.51
Ash chemical compositions (wt%)[a]		
MgO	2.69	ND[b]
Al_2O_3	26.03	21.76
SiO_2	56.34	55.86
SO_3	6.07	4.89
K_2O	1.30	1.96
CaO	4.80	9.91
TiO_2	0.77	0.78
Fe_2O_3	1.97	4.84

[a] Ashes were prepared according to GB/T/212-2008. [b] ND = not detected.

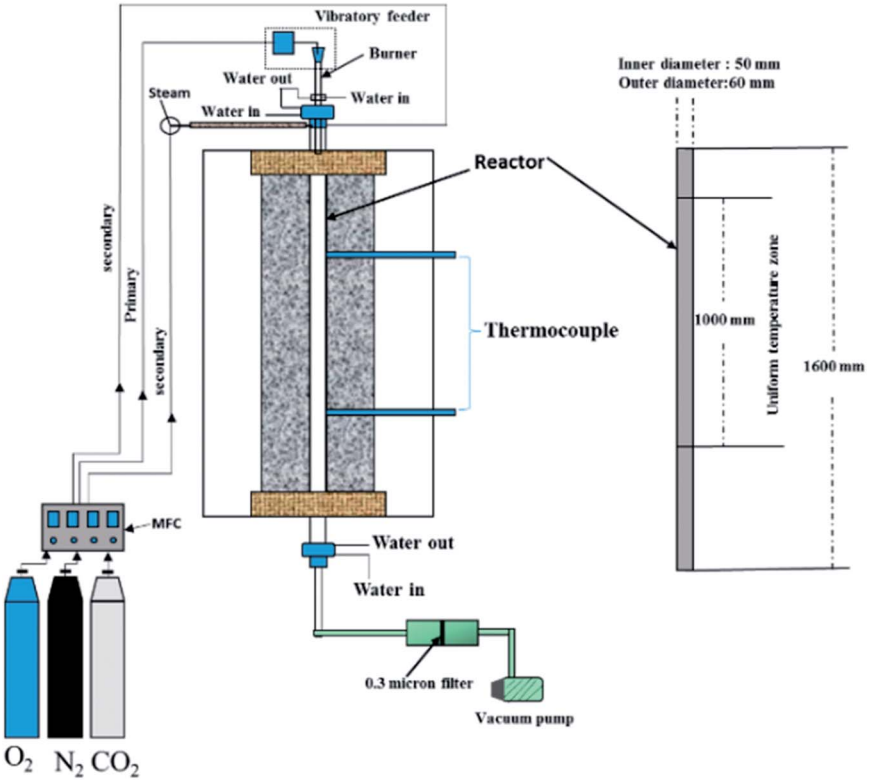

Fig. 1 Experimental system used in this study.

outer diameter of 60 mm and a length of 1600 mm. Water-cooled tubes are installed at the inlet and outlet of the corundum tube to rapidly cool and condense residual coal ash and exhaust gas and to prevent overheating of other external instruments. O_2, N_2 and CO_2 in the gas supply system were injected into the high-temperature furnace using control gas mass flow meters. The water vapors are generated using a constant flow water pump which controls the water flow and converts water into water vapors. Water vapor, and O_2 and CO_2 gas mixtures are carried into the corundum tube reactor. The sample collection system consists of a 0.3 μm porous filter and a vacuum pump (Leybold Sogevac SV25), and the final ash sample is collected from the filter. Micro-vibrator feeder of SANCI (Japan) mixes the pulverized coal with primary air, and then puts it into the furnace reactor. The secondary air supply for burnout is divided into two streams into the reactor, one of which carries gas into the furnace reactor containing water vapor. The feeding rate is about 0.2 g min^{-1}. The whole combustion gas flow rate (primary and secondary air) is 4.5 L min^{-1}, and the primary gas flow rate is 0.6 L min^{-1}. Water vapor is heated at a temperature of 150 °C, then the distribution of the gas flow rate calculations is conducted at 150 °C condition. In the carbon loss test of the residual ash, the burnout rate of the combustion coals in this work is calculated to be less than 1%, that is, the coals are almost completely burned out. The residual time of pulverized coal particles in the furnace is about 1.25 s for all experimental conditions in this work, and it was maintained by adjusting the total gas fed into the reactor system.

For the combustion experiments in this study, four different atmospheres were used to simulate the main air combustion consisting of (21% O_2/79% N_2, and abbreviated as AIR); others included the oxy-fuel combustion OXY21 (21% O_2/79% CO_2), oxy-fuel combustion with high partial oxygen pressure OXY30 (30% O_2/70% CO_2) and H_2O-containing oxy-fuel combustion WOXY30 (10% H_2O/30% O_2/60% CO_2). For reproducibility, each experiment was conducted three times under the same experimental conditions.

2.3. Analysis

Solid products were analysed using XRD, Mössbauer spectroscopy, particle size analyser and SEM-EDX.

XRD analysis was performed using a Dutch PANalytical B.V. X'Pert PRO X-ray device, a copper target ($K\alpha_1 = 0.1542$ nm), in the scan range of 20° to 80° at 40 kV and 40 mA operating conditions. X'Pert HighScore software was used to analyse the diffraction peak.

Mössbauer test was performed at room temperature using an iso-accelerated transmission method, with Pd as the base of the ^{57}Co, α-Fe foil-calibrating spectrometer speed, and the reported isomer shift. The measured spectral lines were calculated using Lorentzian least-squares curve fitting of the spectrum, and then the characteristics of the various components of Mössbauer spectrum parameters, such as isomeric shift (IS), four class splitting (QS) and magnetic hyperfine field (MHF) characteristic parameters were obtained through the so-called "fingerprint" effect and were compared with the parameters in the literature

to determine the iron phase in the sample.[2,4,12] The iron content of each iron-containing phase was determined from the area under the related absorption peak and the data uncertainty analysis was also performed from the fitting curve.[12]

The particle size distribution in the solid products was determined using the Malvern particle size analyser (Mastersizer 2000), which could test the particle size in the particle range of 0–2000 μm.

The surface morphology and chemical compositions of combustion solid products were performed using a Quanta 200 environmental scanning electron microscope equipped with a GENESIS energy dispersive X-ray spectrometry (SEM-EDX).

3. Results and discussion

3.1. Main minerals and Fe-mineral distribution in coal

XRD analysis was used to analyze the mineral phases in experiment coals, as shown in Fig. 2. The results derived from Fig. 2 show that both coal samples contain quartz. In addition, the diffraction peaks of XJC are mainly consisting of kaolinite, quartz and dolomite. The XJC sample is a kind of bituminous coal with medium ash content. Therefore, diffraction peaks of other minerals appeared as well in the XRD pattern. By analogy, diffraction peaks in the XRD pattern of SHC also revealed the presence of other minerals; quartz, kaolinite, ankerite and calcite were the main mineral phases that were detected.

The iron-bearing phases in XJC and SHC samples were further analysed in detail by using Mössbauer spectroscopy (as shown in Fig. 3), and the content of each iron phase was fitted and calculated appropriately. The iron-bearing phases of XJC

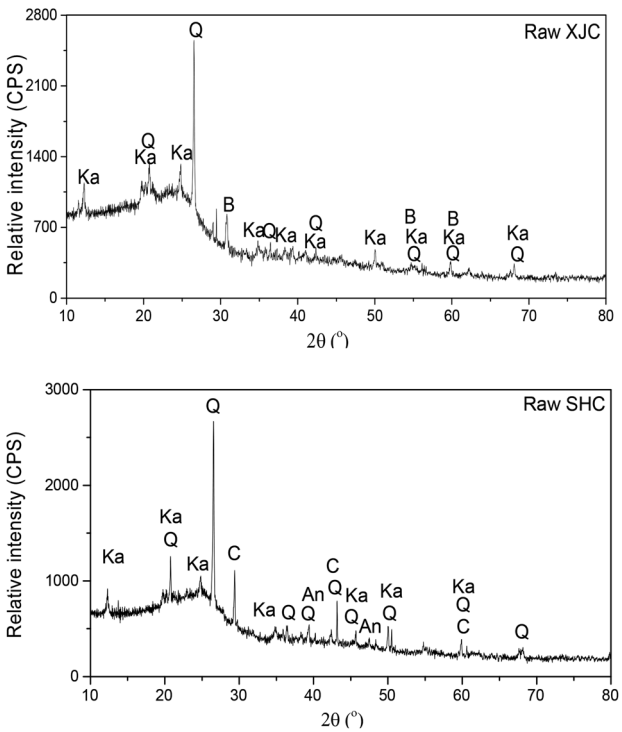

Fig. 2 XRD patterns of raw XJC and SHC samples (Q: quartz; Ka: kaolinite; B: dolomite; An: ankerite; C: calcite).

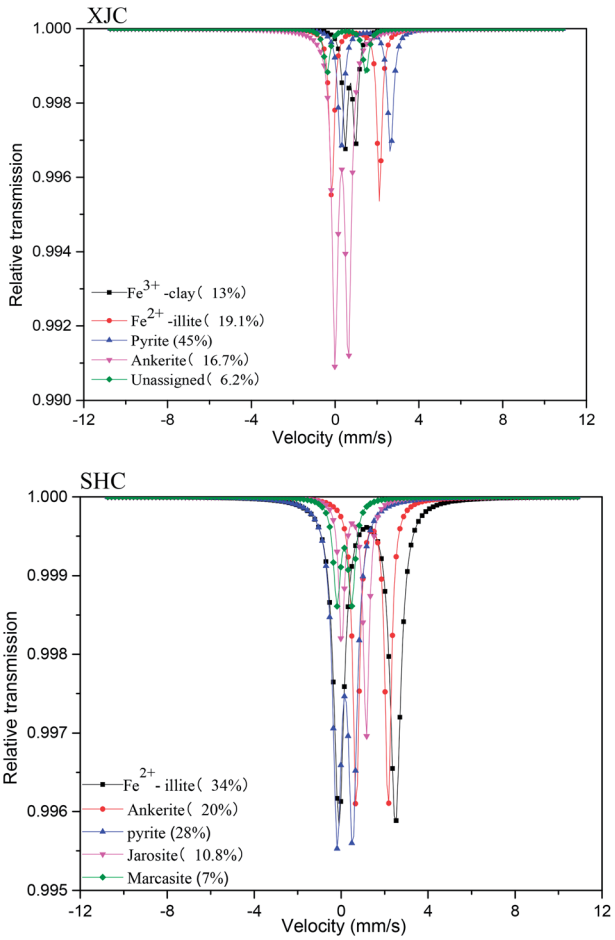

Fig. 3 The Mössbauer spectra of raw coals XJC and SHC.

are mainly due to Fe^{3+}-clay minerals, Fe^{2+}-illite, pyrite and ankerite. The iron content of pyrite, clay minerals and carbonate was estimated to be 45% to 32.1%, and 16.7%, respectively, while a small amount (6.5%) of iron phases remained unclassified.

In the case of the SHC sample, the iron phases are Fe^{2+}-illite, pyrite, ankerite and jarosite. The iron content in the ferrous sulphide phase accounts for 35% of the total iron. This amount is approximately the same (34%) in the iron-containing clay minerals and significantly lower for jarosite (10.8%). In general, the oxidation of pyrite, during coal weathering, storage and transportation affords $XFe_3(OH)_6(SO_4)_2$ (jarosite), where X stands for H^+, K^+, Na^+ or NH_4^+.[26,27]

3.2. Mineral phases of ashes produced from DTF experiments

The XRD patterns of XJC and SHC ashes formed under four different combustion atmospheres are shown in Fig. 4. The XRD analyses of the ashes formed during the XJC combustion show diffraction peaks that do not differ substantially. Apparently, the change of combustion atmospheres from AIR to OXY21, OXY30 and WOXY30 did not significantly alter the formation of crystalline mineral phases in ashes. This means that the oxy-fuel atmosphere (change of oxygen partial pressure or

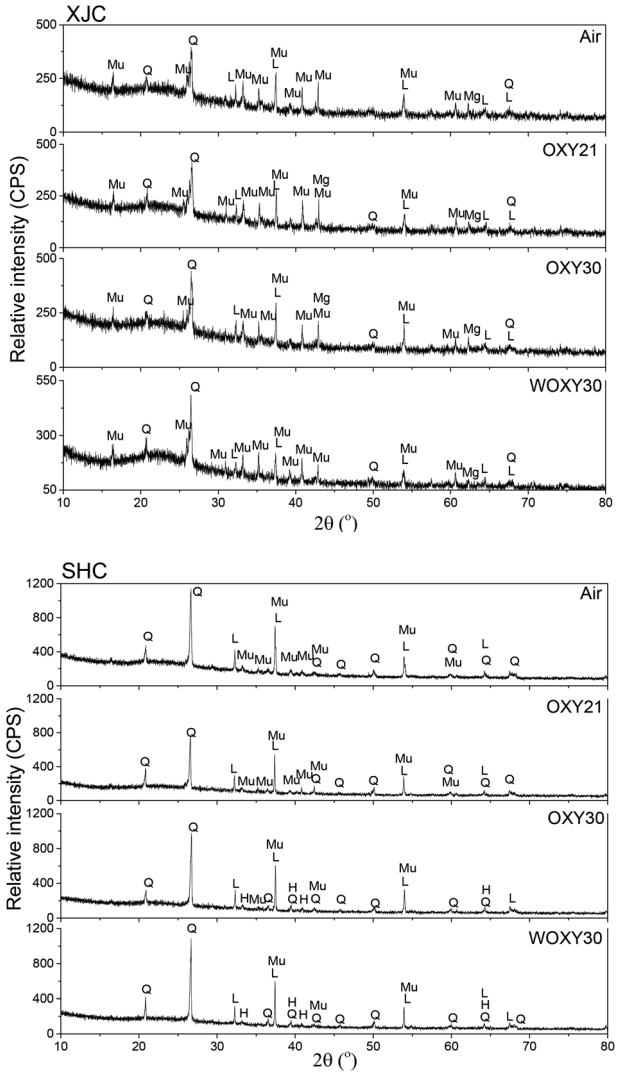

Fig. 4 XRD patterns of XJC and SHC ashes produced from different combustion atmospheres (L: lime; H: hematite; Q: quartz; Mu: mullite; Mg: periclase).

addition of water vapor) did not affect the conversion mechanism of major minerals in coal.[12] The main mineral phases in the ash (XJC sample) are mullite, quartz, lime and calcite. Mullite and quartz are converted from kaolinite and quartz, and lime and calcite are converted from dolomite.

For SHC, however, the main mineral phases of ash formed under air combustion are mullite, lime and quartz. In O_2/CO_2 atmosphere, the crystalline mineral phases are the same as those under the O_2/N_2 atmosphere, although the diffraction peak intensity of each mineral phase is relatively smaller. When the oxygen concentration increases to 30%, the diffraction peak of hematite appears in the ash.

3.3. Fe-containing phases of ashes produced from DTF experiments

The presence of the iron-bearing phase in the ash is a rather complicated issue, including also the iron-oxide phases and the iron-bearing glassy (Tables 2 and 3). From Tables 2 and 3, it can be seen that the type of iron phase remains the same within the four different combustion atmospheres, but the iron distribution in each phase is different. It can be seen from Tables 2 and 3 that the Fe^{3+}-glass silicates are the main parts of the glass phase in the ashes, while Fe^{2+}-glass silicates are only a small part of the iron content in the ashes. The main reason is that the oxygen partial pressure of the furnace gas used in the DTF experiment, in this work, is very high.

For the XJC sample, the iron phase's characteristics in the coal ash collected under different combustion atmospheres are shown in Table 2. The iron phases in all the residues are the same, including the Fe-glass phase, hematite (Fe_2O_3) and magnetite (Fe_3O_4). Tetrahedral magnetite and octahedral magnetite, two different structures of magnetite, can be detected in some ash samples. According to different Mössbauer parameters, the Fe-glass phase includes Fe^{2+}-glass and Fe^{3+}-glass silicates. Low temperature eutectic Fe-glass phases are easy to adhere to the initial sedimentary layer, which is one of the main factors that aggravate slag formation. Table 2 shows that the different combustion atmospheres do not affect the formation of iron-bearing phases in ashes, but they do affect the relative iron content of each Fe-bearing phase. In other words, replacing the combustion atmosphere with O_2/CO_2, increasing the partial oxygen pressure in O_2/CO_2 and adding a certain amount of water vapor will not affect the main path of iron mineral transformation, but they can affect the content of the corresponding iron combustion products.

According to the analysis data presented in Table 2, it is obvious that the change of combustion conditions can significantly change the content of the Fe-bearing phase, thus affecting the transformation of the iron phase. The portions of the Fe-glass phase, hematite and magnetite in Fe-containing phases were further compared for all the experimental

Table 2 ^{57}Fe MÖssbauer analysis of the XJC ashes

XJC sample	IS (mm s^{-1})	QS (mm s^{-1})	M.H.F (kOe)	Fe (%)	Fe phase
AIR	0.91	2.03		7.2	Fe^{2+}-glass
	0.28	1.28		25.4	Fe^{3+}-glass
	0.37	0.09	513	26.2	Hematite
	0.29	0.05	488	11.1	Magnetite[a]
	0.47	0.01	448	30.1	Magnetite[b]
OXY21	0.57	2.45		9	Fe^{2+}-glass
	0.32	1.13		23.8	Fe^{3+}-glass
	0.37	−0.1	514	29.6	Hematite
	0.37	−0.02	488	12.6	Magnetite[a]
	0.45	−0.03	431	25	Magnetite[b]
OXY30	0.93	1.88		5.8	Fe^{2+}-glass
	0.27	1.14		27.8	Fe^{3+}-glass
	0.37	−0.09	514	33.3	Hematite
	0.34	−0.05	489	24.1	Magnetite[a]
	0.39	−0.1	447	9	Magnetite[b]
WOXY30	0.73	2.48		5.4	Fe^{2+}-glass
	0.33	1.16		26.8	Fe^{3+}-glass
	0.36	−0.08	513	34.3	Hematite
	0.41	−0.03	479	33.5	Magnetite[a]

[a] Tetrahedral. [b] Octahedral.

Table 3 ^{57}Fe MÖssbauer analysis of the SHC ashes

SHC samples	IS (mm s^{-1})	QS (mm s^{-1})	M.H.F (kOe)	Fe (%)	Fe phase
AIR	0.68	2.54		7.3	Fe^{2+}-glass
	0.36	1.09		37.6	Fe^{3+}-glass
	0.35	−0.07	515	26.1	Hematite
	0.46	−0.05	464	29	Magnetite[b]
OXY21	0.78	2.75		9.2	Fe^{2+}-glass
	0.35	0.98		38	Fe^{3+}-glass
	0.38	−0.08	515	21.8	Hematite
	0.50	0.05	467	31	Magnetite[b]
OXY30	1.05	2.10		6.5	Fe^{2+}-glass
	0.32	1.15		36.7	Fe^{3+}-glass
	0.38	−0.08	516	28.9	Hematite
	0.29	−0.01	492	6.4	Magnetite[a]
	0.41	−0.15	445	21.5	Magnetite[b]
WOXY30	0.95	1.96		5.9	Fe^{2+}-glass
	0.25	1.49		30.2	Fe^{3+}-glass
	0.37	−0.09	516	30.5	Hematite
	0.15	−0.02	496	7.4	Magnetite[a]
	0.51	−0.03	457	26	Magnetite[b]

[a] Tetrahedral. [b] Octahedral.

atmospheres studied, and the results are shown in Fig. 5. Obviously, for XJC ash samples, most Fe is present in the magnetite form, followed by the Fe-glass phase, and hematite is the least. Compared with the air atmosphere sample (AIR), in the oxy-fuel combustion atmosphere, with the same partial oxygen pressure, the relative content of Fe-glass in the ashe is almost the same. The amount of hematite is increased and that of magnetite is decreased. These results are in accordance with the previously reported investigation of Yu *et al.*,[2] in which they speculated that almost all iron-containing minerals pyrite in coal that are particles in the combustion process is transformed all alone into iron oxides. Thus, the pyrite particles are almost impossible to contact other particles within aluminum silicates. The amount of Fe-glass silicates converted from iron-bearing clay minerals is not affected by the combustion atmosphere. From the data shown in Fig. 5, we realize that the iron glass phases in the ashes are almost not affected by the combustion atmosphere, compared with raw coal iron minerals reported in Section 3.1. In addition, the content of Fe-glass in the ashes formed from the clay minerals and Fe^{2+}-illite is similar to the content of clay minerals and Fe^{2+}-illite in the raw coal during the four different combustion atmospheres, suggesting that in the XJC sample, pyrite and iron carbonate could mainly be excluded.

The biggest difference between O_2/CO_2 and air combustion atmosphere is that the dilution gas in the reactor changes from N_2 to CO_2. Therefore, differences observed in the formation of Fe-bearing products, under the two combustion atmospheres, could be attributed to the influence of the higher concentration of CO_2. Based on a literature survey performed,[28–31] pyrite in the N_2 atmosphere generally transforms into pyrrhotite, while in the CO_2 atmosphere, magnetite is formed that then turns into hematite. The decomposed products of pyrite may further react with CO_2 to form iron oxides, indicating that CO_2 is further conducive to the transformation of pyrite.[31] The higher heat capacity of CO_2 (ref. 12 and 32) leads to a lower temperature for the combustion of particles in the atmosphere, which is conducive for the transformation of pyrite into hematite.[28] Compared with AIR case OXY21 is conducive to the formation of hematite, due to its lower particle temperature. Since the pyrite decomposition products can react with CO_2 to form iron oxides, OXY21 results mainly in the formation of hematite and magnetite (as shown in Fig. 5).

For the case of O_2/CO_2 combustion OXY30, where the concentration of oxygen was 30%, an increase in the hematite content in the ash was observed, while that in magnetite was decreased. Thus, the CO_2 partial pressure was reduced, and as a consequence, the proportion of the pyrite reacting with CO_2 to form iron oxides was also reduced. It is worth noting that the

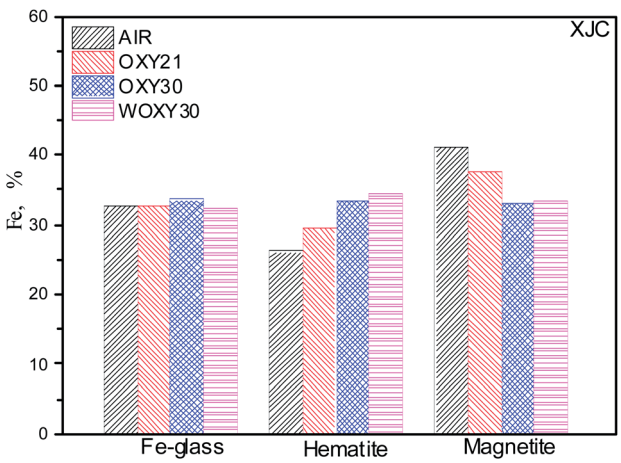

Fig. 5 Iron phase distributions in XJC ashes produced from different combustion atmospheres.

pyrolysis rate of pyrite in the CO_2 atmosphere is fairly small,[28] especially, when the oxygen partial pressure is high. Increasing the oxygen partial pressure is followed by an increase in the ash hematite content. Therefore, we may conclude that the direct oxidation of pyrite to hematite is easier in the OXY30 atmosphere.

Next, a certain proportion of CO_2 (10%) was replaced by water vapor (WOXY30). In this case, Fe-glass phases content in the ash formed from the combustion of pulverized coal was decreased slightly, while the hematite and magnetite contents were increased. Finally, the total iron oxide content was increased as well (shown in Table 2 and Fig. 5). Taken into consideration that the experiment was conducted at a relatively high temperature (1450 °C), we should keep in mind that the diffusion-limited reaction rate will be sensitive to experimental conditions.[16,18] The O_2 concentration of 30% and a low H_2O level are favorable for the establishment of pulverized coal combustion in oxy-fuel combustion atmosphere.[33] On the one hand, water vapor replaces part of the dilute CO_2 gas, and O_2 diffusion is faster in H_2O.[34] Thus, molecular O_2 is more likely to reach the surface of combustion particles and be in close contact with iron minerals in coal to form more iron oxides during the short residence time in the DTF chamber. On the other hand, the combustion particles are more easily fragmented as more oxygen diffuses to the particle surface making it greatly difficult for iron-bearing minerals to be in contact with clay or other silicates included in the particles to form Fe-glass.[2,12,25] Our previously-reported study[34] supported the results presented herein, highlighting that the reaction rate of pyrite in the steam-containing atmosphere to be higher than that in the CO_2-containing atmosphere. In the DTF experiment, the addition of water vapor increases the transformation of octahedral magnetite to tetrahedral magnetite, thus, facilitating the formation of hematite from magnetite.

The iron phases formed during the SHC combustion experiment and in the four different atmospheres were the same as XJC consisting of Fe^{2+}-glass silicate, Fe^{3+}-silicate, hematite and magnetite as shown in Table 3. The portions of the Fe-glass phase, hematite and magnetite in Fe-containing phases were further compared to all experimental atmospheres studied, and the results are shown in Fig. 6. The content of Fe-glass phases is high, approximately reaching a value of 50%, suggesting further that pyrite or iron carbonate, *etc.* in coal particles may form a large proportion of Fe-glass silicates.[21] During the combustion transformation process, a certain proportion of non-clay Fe-containing minerals, pyrite and ankerite exist in the interior of the particles in combination with silicate forming the relevant Fe-glass phases. As the partial pressure of oxygen remains the same, more iron-bearing glass phases and less hematite are formed in the O_2/CO_2 atmosphere. This is mainly due to the different combustion temperatures of char particles in two different atmospheres, which subsequently affect the transformation of iron phases in the particles. Compared with AIR, the lower particle temperature in OXY21 may delay the transformation of internal iron minerals into iron oxides. Intermediate products pyrrhotite of pyrite transformation has a melting temperature of about 1100 °C, and FeO–FeS has a eutectic temperature of about 950 °C, both easily react with internal silicate to form Fe-glass silicates. In addition, the higher concentration of CO in OXY21, can not only delay the transformation of pyrite and other iron-bearing minerals into iron oxides[4,35] but can also reduce the melting temperature of the iron-bearing phase, thus strengthening the formation of the iron-containing glass phases.

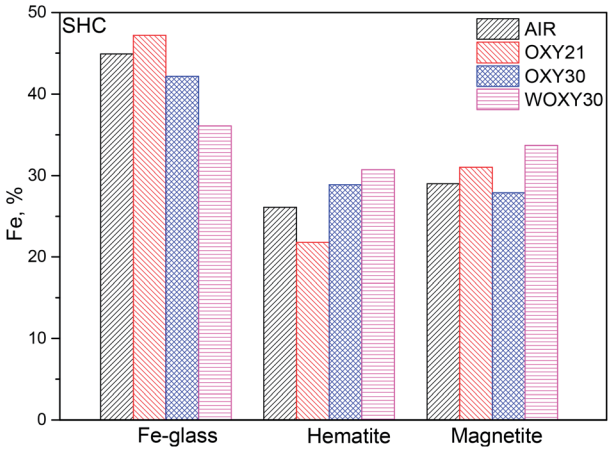

Fig. 6 Iron phase distribution SHC ashes produced from different combustion atmospheres.

As shown in Table 3 and Fig. 6, for the SHC sample, an increase in the oxygen concentration to 30% (in O_2/CO_2 combustion atmosphere) results in a decrease of the Fe-glass phase and magnetite contents in the ash, while the content of hematite increases. Also, an increase in the hematite content in the ash is observed.[2,4] From Table 3, we can also see that Fe^{2+}-glass silicate formed in OXY30 is significantly reduced compared to that in OXY21. For the OXY21 case, with 21% oxygen content and at high temperature, the Fe^{2+}-glass state can be further oxidized to the Fe^{3+}-glass state, however, the diffusion of oxygen through Fe^{2+}-glass silicate may limit the reaction process.[4,36,37] This further suggests that an increase in the O_2 concentration promotes the relative Fe^{2+}-glass state to be converted into a Fe^{3+}-glass state in the combustion environment.

As shown in Fig. 6, in the O_2/CO_2 combustion atmosphere experiment with the same oxygen partial pressure, when 10% of water vapours replaces the diluent CO_2 it results in a significant decrease in the content of Fe-glass phases in the formed ash, while hematite and magnetite contents were increased. Thus, the content of total iron oxides increases. Generally, it is known that O_2 diffuses faster in H_2O than in CO_2 gas.[34] Therefore, during the short residence time in the DTF chamber, O_2 is more likely to reach the surface of combustion particles and be in contact with iron-containing minerals. The data presented in Fig. 6 shows that the content of magnetite is relatively higher, suggesting that some Fe-containing minerals inside the coal are converted to magnetite, and then to hematite.[2,12] We may also suggest that the addition of water vapours does not significantly affect the type of iron phase formed in ashes, although the type and iron content vary with the type of coal.

A comparison of the relative Fe^{3+}-glass to Fe^{2+}-glass ratio of the ashes produced in the four different combustion atmospheres presented in Fig. 7 is in accordance with the literature

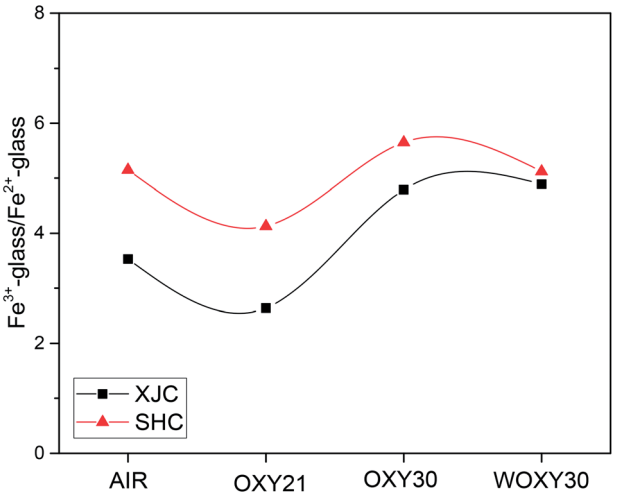

Fig. 7 Fe^{3+}-glass to Fe^{2+}-glass ratio as a function of combustion atmospheres.

reports.[4,36,37] We may suggest that Fe^{3+}-glass is the main glass silicates. The iron-bearing minerals in the studied coals will be transformed to Fe^{2+}-glass in the OXY21 more than that in the AIR, due to the lower char combustion temperatures in O_2/CO_2 atmosphere.[1,12,21] The data also suggest that the 30% increase in oxygen concentration in the combustion atmosphere is followed by an increase of the Fe^{3+}-glass to Fe^{2+}-glass ratio. The amount of oxygen diffused to the combustion particle surface is increased as the oxygen partial pressure increase.[2]

3.4. Particle size distribution of ashes produced from DTF experiments

Malvern laser particle size analyser was used to analyse the raw coal and particle size distribution in ashes, and the results are shown in Fig. 8. Compared to the particle size distribution in raw coal, the sizes of the ash particles produced from AIR, OXY21 and OXY30 move to smaller particle size region. The ashes formed from AIR, OXY21 and OXY30, were in the sub-micron area (0.1–1 μm), while the XJC ash of WOXY30 with a certain amount of water vapor did not form particles in the sub-micron area. Generally, combustion particles form three ash particle size regions,[38] ranging from sub-micron to 10 μm and 100 μm size region. The formation of sub-micron particles is mainly caused by the evaporation and condensation mechanism,[39] while the formation of particles sizes greater than 10 microns is mainly ascribed to particle fragmentation including minerals agglomeration.[40] There is no obvious difference in the ash particle size distributions under combustion conditions without steam. This result is in accordance with the results of Sheng *et al.*[38] and Wall *et al.*[41]

The particle size distributions in ashes produced under O_2/CO_2 and O_2/N_2 atmospheres are further compared. There is a significant difference in the 10 μm particle distribution area (as seen in Fig. 8). Different types of coal have different effects on the ash particle size distribution. In fact, the XJC ash sample affords a higher amount of ash particles with particle size less

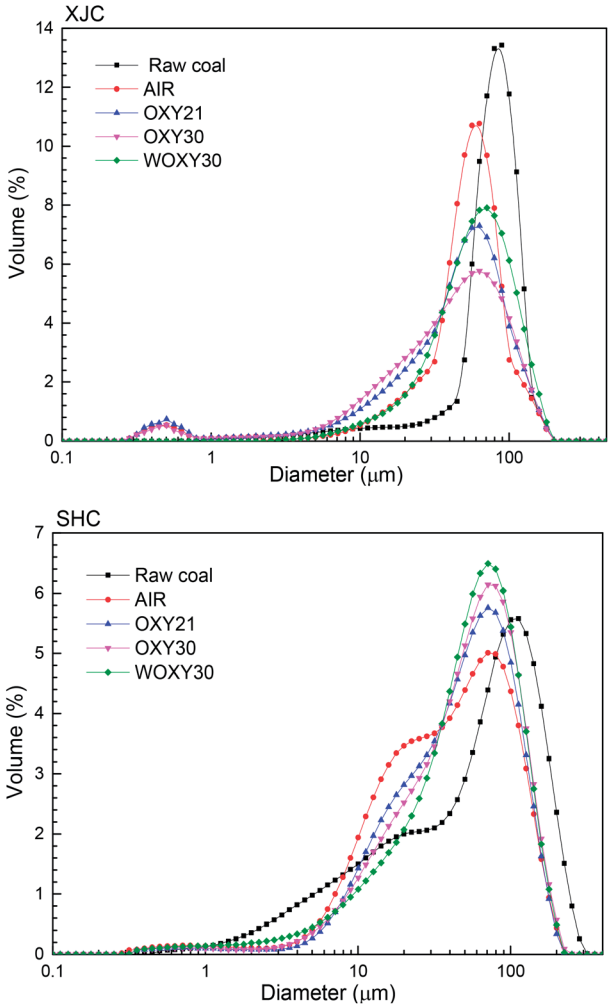

Fig. 8 Size distributions of XJC and SHC ashes and raw coals.

than 10 μm, while SHC forms significantly less (in O_2/CO_2 combustion atmosphere) amount of particles in that size range. This is most likely due to fragmentation and agglomeration of minerals in the coal during the combustion process as fragmentation competes with agglomeration at the same time, resulting in different effects of the atmosphere on different types of coal. In the O_2/CO_2 atmosphere, the higher CO_2 heat capacity and the lower diffusion rate of O_2 in CO_2 (ref. 31 and 42) leads to lower temperatures of the char particles. As a result, the fragmentation and agglomeration of minerals are obviously affected. In addition, both processes are also highly dependent on intrinsic characteristics such as particle size and type of the coal particles. In fact, the combustion temperature and the mineral transformation behaviour of char particles vary within different coals studied.

From Fig. 8, we can clearly see that when a certain amount of water vapour is added to the combustion atmosphere XJC or SHC, (WOXY30 case), the amount of ash particles formed with a size of lower than 10 μm is relatively low. On the other hand, when a certain portion of CO_2 in the atmosphere is replaced by H_2O, it is beneficial to reduce the formation of ash particles with particle sizes less than 10 μm. Practically, the formed ash

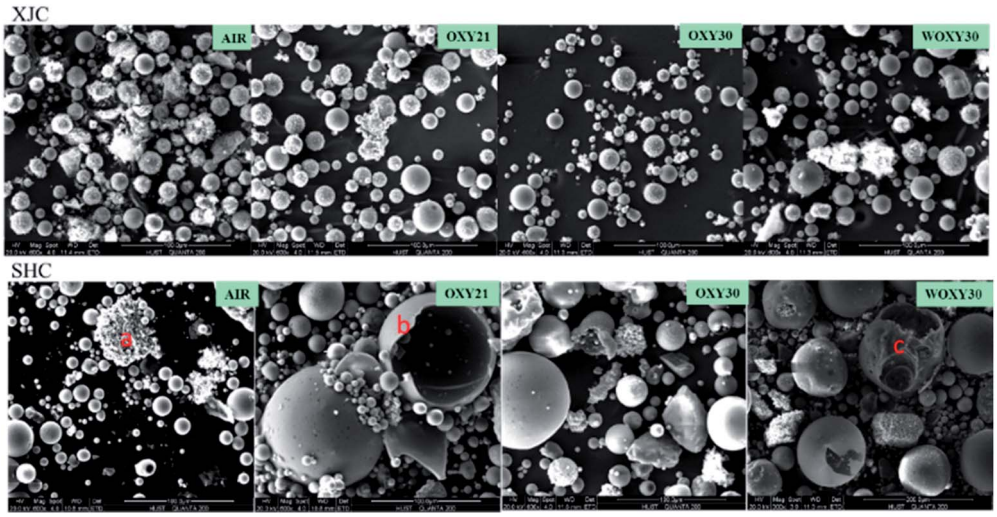

Fig. 9 SEM images of XJC and SHC ashes produced in different combustion atmospheres.

particles move to the larger particle size region (10–100 μm), suggesting that more ash particles fall into the bottom of the ash due to gravity, which might decrease the deposition and slagging propensity of coal ash on the heat transfer surface.

3.5. Microstructure and chemical composition of ash particles produced from DTF experiments

The morphology of the bulk ashes is shown in Fig. 9. The ash particle size observed in the images ranges from less than 1 μm to greater than 100 μm, which is in accordance with the results reported earlier in Section 3.4. Morphologies of the ash particles vary and mainly consist of solid spheres (cenospheres) and amorphous particles. It can be seen from the images of XJC that the morphologies of ash particles are quite similar in the four different combustion atmospheres studied. This further suggests that the combustion atmosphere does not significantly affect the ash morphology. However, in SHC images, and the morphologies of the ash particles are different. According to the microstructural characteristics, SHC ash particles consist of many other bigger particles, exhibiting agglomerate morphology (particle a), cracked hollow spheres (particle b) and molten hollow spheres (particle c).

The chemical composition of a single ash particle was further determined by SEM-EDX techniques and is shown in Fig. 10. The ash particles from XJC contain many granular spheres (Fig. 10A) and smooth spheres (Fig. 10B). In addition, EDX spectra show that the predominant elements are mainly Ca, Al, Mg, Si and S in the granular spheres and Si, Al, Na and K in the smooth spheres, as referred to in literature reports.[43,44] Finally, for the XJC ash, results suggest that the Fe-containing minerals are mainly present as excluded minerals transformed independently and hardly in contact with other minerals.

From SHC ash, two kinds of typical ash particles are seen as shown in Fig. 10C and D. The EDX spectra in Fig. 10C show that the cracked cenospheres at the internal surface mainly contain Si, Al, K, Ca and Fe. The external surface, on the other hand, contains Si, Al, and K, which also suggests that rather a small amount of Fe-containing mineral is in contact with Ca-containing minerals and clay minerals inside the particle. The ash particles presented in Fig. 10D are not completely spherical. They contain big holes filled with some smaller spheres inside (plerospheres). EDX analysis also shows that the iron content inside the particle (spectrum a in Fig. 10D) is lower than that outside the particle (spectrum b in Fig. 10D). However, the Si–Al content is higher inside the particle and lower outside, suggesting that plerospheres in SHC ashes are formed from the complex eutectics of internal iron-bearing minerals and clays.[45] This also is speculation that the iron-bearing mineral (pyrite, ankerite, *etc.*) in SHC is mostly included in nature.

4. Conclusions

The work presented here has led to the following results. The mineral crystallites in the ashes formed under different atmospheres are almost the same for coal samples studied in the work, and a change in the combustion atmosphere does not significantly affect the transformation of the major minerals in the coal. Mössbauer analysis reveals that the iron-bearing phases in the residual ashes include Fe-glass phases, hematite and magnetite. The change of combustion atmosphere can affect the relative content of iron phases in the ashes. Compared with air combustion, the Fe^{3+}-glass to Fe^{2+}-glass ratio is significantly decreased in O_2/CO_2 combustion atmosphere. For the XJC ash, O_2/CO_2 combustion is conducive to hematite formation, while it has no impact on the formation of the Fe-glass phase; for the SHC ash, O_2/CO_2 atmosphere results in more iron melting into Fe-glass phases and less iron oxide formation. Replacing a certain portion of CO_2 with H_2O and increasing O_2 concentration promotes iron oxide formation. In O_2/CO_2 combustion atmosphere with the same oxygen partial pressure, the addition of water vapour results in the size of ash particles that moves towards the larger particle size regions. The Fe-containing minerals in XJC ash are mainly present as excluded minerals transformed independently while in the SHC

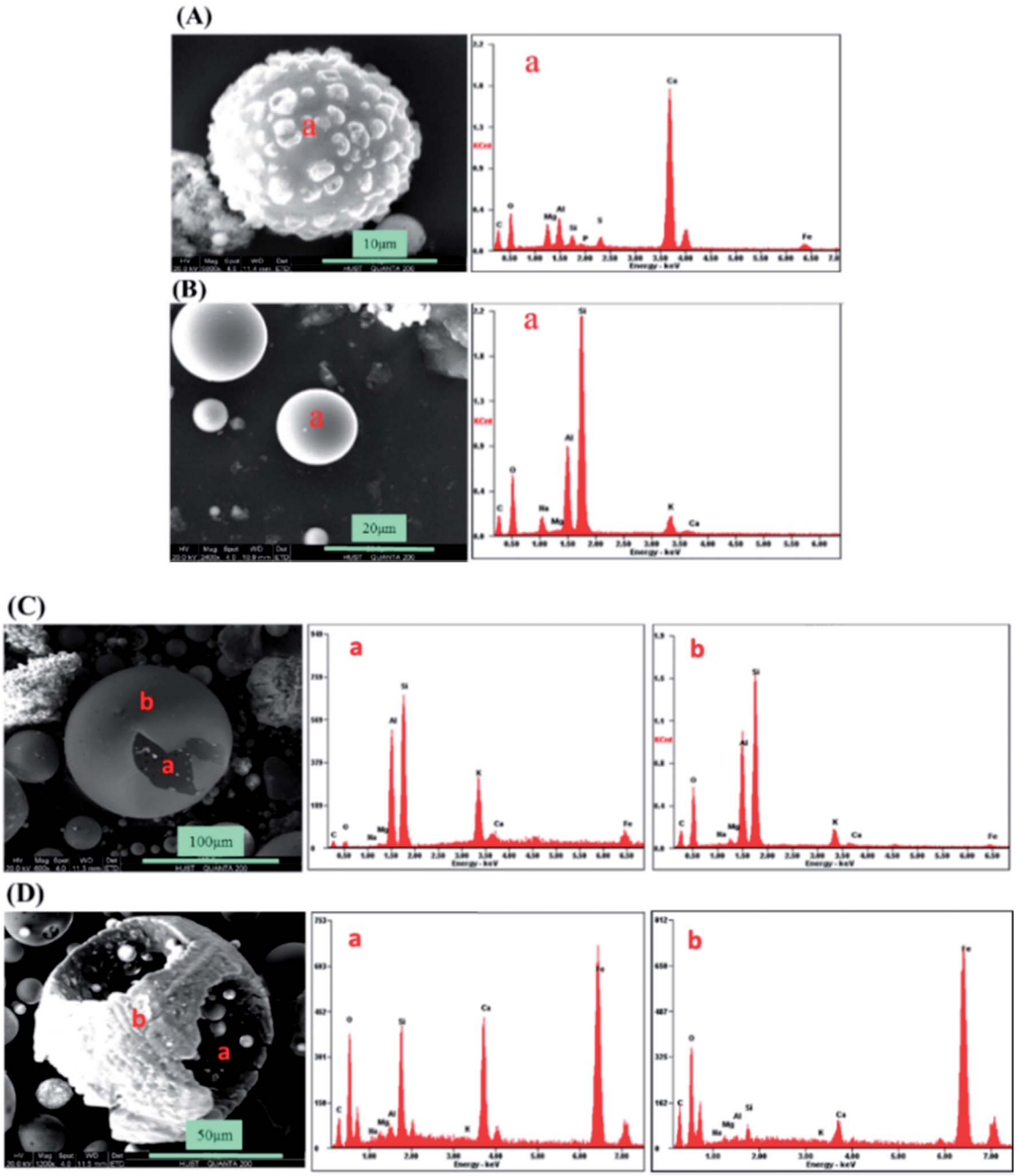

Fig. 10 SEM images and EDX spectra of ash particles. Ash particles from XJC (A and B), ash particles from SHC (C and D), respectively.

ash, the Fe-containing minerals are mostly included in nature, transformed significantly affected by combustion atmosphere.

Conflicts of interest

There are no conflicts to declare.

Acknowledgements

This work was supported by the National Natural Science Fund Program of China (51706085).

References

1 J. L. Sheng, Y. Li and C. Wang, *Asia-Pac. J. Chem. Eng.*, 2010, **5**(2), 304–309.
2 D. Yu, L. Zhao, Z. Zhang, C. Wen, M. Xu and H. Yao, *Energy Fuels*, 2012, **26**(6), 3150–3155.
3 D. Shu, T. Chen, X. Zou, M. Li, C. Wang, H. Wang, Z. Han and H. Liu, *Sci. Total Environ.*, 2020, **731**, 138951.
4 T. Zeng, J. J. Helble, L. E. Bool and A. F. Sarofirm, *Fuel*, 2009, **88**(3), 566–572.
5 S. Srinivasachar, J. J. Helble and A. A. Boni, *Prog. Energy Combust. Sci.*, 1990, **16**(4), 281–292.

6 L. L. Baxter and R. E. Mitchell, *Combust. Flame*, 1992, **88**(1), 1–14.
7 C. L. Senior and S. Srinivasachar, *Energy Fuels*, 1995, **9**(2), 277–283.
8 L. E. Bool, T. W. Peterson and J. O. L. Wendt, *Combust. Flame*, 1995, **100**(1), 262–270.
9 H. M. Brink, S. Eenkhoorn and M. Weeda, *Fuel Process. Technol.*, 1996, **47**(3), 233–243.
10 B. Dai, X. Wu, J. Zhang, Y. Ninomiya, D. Yu and L. Zhang, *Fuel*, 2020, **264**, 116855.
11 C. W. Bailey, G. W. Bryant, E. M. Matthews and T. F. Wall, *Energy Fuels*, 1998, **12**(3), 464–469.
12 C. Sheng and Y. Li, *Fuel*, 2008, **87**(7), 1297–1305.
13 G. Krishnamoorthy and J. M. Veranth, *Energy Fuels*, 2003, **17**(5), 1367–1371.
14 M. Anheden, U. Burchhardt, H. Ecke, R. Faber, O. Jidinger, R. Giering, H. Kass, S. Lysk, E. Ramström and J. Yan, *Energy Procedia*, 2011, **4**, 941–950.
15 R. Payne, S. L. Chen, A. M. Wolsky, *et al.*, *Combust. Sci. Technol.*, 1989, **67**(1–3), 1–16.
16 I. Guedea, I. Bolea, C. Lupiáñez, N. Cortés, E. Teruel, J. Pallarés, L. I. Díez and L. M. Romeo, *Energy Procedia*, 2011, **4**, 972–979.
17 S. Seepana and S. Jayanti, *Energy Convers. Manage.*, 2010, **51**(10), 1981–1988.
18 Z. Mao, L. Zhang, X. Zhu, C. Pan, B. Yi and C. Zheng, *Appl. Energy*, 2016, **161**, 112–123.
19 Y. Wang and D. A. Bell, *Fuel*, 2017, **187**, 94–102.
20 S. Yadav and S. S. Mondal, *Fuel*, 2020, **271**, 117611.
21 Y. Niu, S. Liu, C. R. Shaddix and S. Hui, *Proc. Combust. Inst.*, 2019, **37**(3), 2781–2790.
22 C. K. Stimpson, S. Chamberlain and D. R. Tree, *Combust. Sci. Technol.*, 2013, **185**(7), 1098–1117.
23 Z. Zhan, C. Andrew, M. Zhou, K. Davis, D. Wang, J. Beutler, M. Cremer, Y. Wang and J. O. L. Wendt, *Proc. Combust. Inst.*, 2020, DOI: 10.1016/j.proci.2020.06.073.
24 Y. Niu, S. Wang, C. R. Shaddix and S. Hui, *Combust. Flame*, 2016, **173**, 195–207.
25 Z. Zhan, L. Bool, E. Andrew, A. Fry, W. Fan, M. Xu, D. Yu and J. O. L. Wendt, *Energy Fuels*, 2013, **28**(1), 146–154.
26 R. A. Creelman and C. R. Ward, *Int. J. Coal Geol.*, 1996, **30**(3), 249–269.
27 S. V. Vassilev and C. G. Vassileva, *Fuel Process. Technol.*, 1996, **48**(2), 85–106.
28 G. Hu, D. J. Kim, S. Wedel and J. P. Hansen, *Prog. Energy Combust. Sci.*, 2006, **32**(3), 295–314.
29 S. K. Bhargava and N. D. Subasinghe, *Fuel*, 2009, **88**(6), 988–993.
30 M. G. Aylmore and F. J. Lincoln, *J. Alloys Compd.*, 2000, **309**(1), 61–74.
31 F. Huang, L. Q. Zhang, B. J. Yi, Z. J. Xia and C. G. Zheng, *Fuel Process. Technol.*, 2015, **138**, 814–824.
32 L. Chen, S. Z. Yong and A. F. Ghoniem, *Prog. Energy Combust. Sci.*, 2012, **38**(2), 156–214.
33 Z. Zhang, X. Li, L. Zhang, C. Luo, B. Lu, Y. Xu, J. Liu, A. Chen and C. Zheng, *Fuel Process. Technol.*, 2019, **184**, 27–35.
34 F. Huang, L. Zhang, B. Yi, Z. Xia and C. Zheng, *Fuel Process. Technol.*, 2015, **131**, 458–465.
35 G. P. Huffman, F. E. Huggins and G. R. Dunmyre, *Fuel*, 1981, **60**(7), 585–597.
36 S. Srinivasachar and A. A. Boni, *Fuel*, 1989, **68**(7), 829–836.
37 R. F. Cooper, J. B. Fanselow and J. K. R. Weber, *Science*, 1996, **274**(5290), 1173–1176.
38 C. Sheng, Y. Li, X. Liu, H. Yao and M. Xu, *Fuel Process. Technol.*, 2007, **88**(11), 1021–1028.
39 J. S. Lighty, J. M. Veranth and A. F. Sarofim, *J. Air Waste Manage. Assoc.*, 2000, **50**(9), 1565–1618.
40 W. P. Linak and J. O. L. Wendt, *Fuel Process. Technol.*, 1994, **39**(1), 173–198.
41 T. F. Wall, E. L. Khare, S. Liu, Y. Yamada and T. Tamura, in *Proceedings: impacts of fuel quality on power production*, Utah, USA, 2006.
42 A. Molina and C. R. Shaddix, *Proc. Combust. Inst.*, 2007, **31**(2), 1905–1912.
43 Y. Zhao, J. Zhang and C. Zheng, *Int. J. Coal Geol.*, 2012, **94**, 182–190.
44 Y. Zhao, J. Zhang, C. Tian, H. Li, X. Shao and C. Zheng, *Energy Fuels*, 2010, **24**(2), 834–843.
45 Y. Zhao, J. Zhang, J. Sun, X. Bai and C. Zheng, *Energy Fuels*, 2006, **20**(4), 1490–1497.